ARTICLE

Low-Temperature Synthesis of $CuInSe_2$ Nanotube Array on Conducting Glass Substrates for Solar Cell Application

Jun Xu,[†] Chun-Yan Luan,[†] Yong-Bing Tang,[†] Xue Chen,[†] Juan Antnio Zapien,[†] Wen-Jun Zhang,[†] Hoi-Lun Kwong,[‡] Xiang-Min Meng,[§,*] Shuit-Tong Lee,[†] and Chun-Sing Lee[†,*]

[†]Center of Super-Diamond and Advanced Films (COSDAF), Department of Physics and Materials Science and [‡]Department of Biology and Chemistry, City University of Hong Kong, Hong Kong SAR, People's Republic of China and [§]Key Laboratory of Photochemical Conversion and Optoelectronic Materials, Technical Institute of Physics and Chemistry, CAS, Beijing 100101, People's Republic of China

ABSTRACT Highly ordered arrays of Cu-rich and -deficient $CuInSe_2$ nanotubes as well as ZnO/$CuInSe_2$ core/sheath nanocables have been synthesized on glass substrates by using ZnO nanorod arrays as sacrificial templates *via* a low-cost solution method. Chemical conversions from hexagonal ZnO to cubic ZnSe, hexagonal CuSe and tetragonal $CuInSe_2$ are demonstrated as a novel means for synthesis of I—III—VI nanomaterials. Large differences in their solubility product constant (K_{sp}) are crucial for direct exchange in the conversions. In solvothermal reaction of ZnO/CuSe core/shell nanocables with $InCl_3$, the triethylene glycol solvent serves as a reducing agent for the reduction of cupric (Cu^{2+}) to cuprous (Cu^{+}) ions and also as an agent for the dissolution of ZnO cores. The absorption coefficient of the $CuInSe_2$ nanotubes in the visible region is on the order of 10^4 cm^{-1}. Photoelectrochemical solar cells were fabricated with arrays of ZnO/$Cu_{1.57\pm0.10}In_{0.68\pm0.10}Se_2$ and ZnO/CuSe nanocables. It was found that power conversion efficiency of the ZnO/$Cu_{1.57\pm0.10}In_{0.68\pm0.10}Se_2$ cell is about two times higher than that based on ZnO/CuSe.

KEYWORDS: $CuInSe_2$ · CuSe · core/shell · nanocables · sacrificial · templates · ions · changes · polyol · reduction

Due to their unique structural and outstanding optoelectronic properties, such as controllable energy band gap by incorporation of Ga and/or S, high absorption coefficient, and long-term stability, chalcopyrite copper indium selenide (CIS) and related materials ($CuInSe_2$, $Cu(In_xGa_{1-x})Se_2$, $CuIn(S_xSe_{1-x})_2$) have been considered to be promising alternatives to polycrystalline silicon for photovoltaic applications.[1−5] While high-power conversion efficiency of about 20% has been demonstrated in polycrystalline $Cu(In_xGa_{1-x})Se_2$ (CIGS) thin film solar cell,[6,7] its wide applications have not yet been realized. This is mainly due to the relatively high manufacturing cost involved in their vacuum coevaporation/sputtering processes, the difficultly in achieving controllable and uniform composition over a large area, and the toxic environment involved on using Se or H_2Se gases.[6−9] Recently a low−cost coating technique has been developed to fabricate CIGS nanocrystals films on transparent conducting substrates. In this process, CIGS nanocrystals were first dispersed in solvents to create paints for coating onto substrates to form CIGS films upon heat treatments.[10−12] However, energy conversion efficiency of devices based on such films is rather low due to high serial resistances attributed to poor electrical contacts between the CIGS nanocrystals and the substrate. One possible approach to alleviate this problem is to directly grow CIGS nanostructures on transparent conducting substrates.

Arrays of one-dimensional (1D) core/shell nanocables have recently attracted intense attention and are considered as promising structures for photovoltaic applications as they may rival traditional planar solid-state p−n junction devices and nanocrystalline dye-sensitized solar cells in three aspects: (i) Arrays of 1D nanostructures often have superior optical absorption due to their light-scattering and -trapping morphologies;[13] (ii) Core/shell nanocables provide an additional advantage of large donor/acceptor junction area. Their unique geometry allows long enough cable lengths for adequate light absorption, while ensuring all photogenerated charge carriers are close to the acceptor/donor junction.[14,15] (iii) Core/shell nanocables provide direct 1D conduction pathways enabling efficient charge transport along the cables.[14,16,17] For example, arrays of ZnO/CdTe core/shell nanocables on indium−tin oxide (ITO) glass substrates have been synthesized and used as photoelectrodes for solar energy applications, yielding a photocurrent density of 5.9 mA cm^{-2} under AM 1.5G illumination with an intensity of 100

*Address correspondence to apcslee@cityu.edu.hk, xmmeng@mail.ipc.ac.cn.

Received for review June 28, 2010 and accepted September 28, 2010.

Published online October 6, 2010. 10.1021/nn101467p

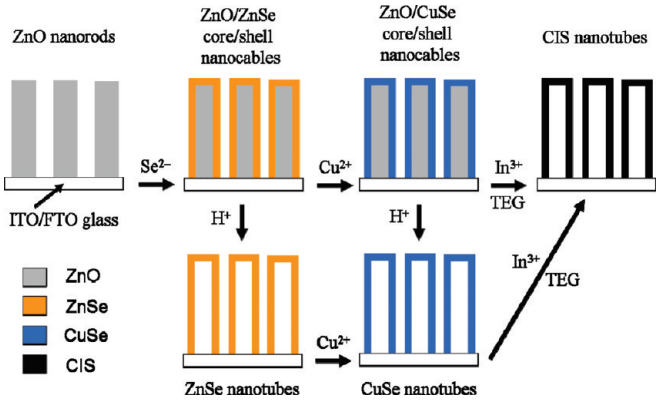

Scheme 1. Schematic illustration for the formation process of the CIS nanotube arrays.

mW cm^{-2}.[18] Yang *et al*. have demonstrated solar cells based on n−p core−shell silicon nanocable arrays with short circuit current and power conversion efficiency reaching 4.28 mA cm^{-2} and 0.46% respectively under 1 sun illumination.[16] They also reported that high-density Si/TiO_2 core/shell nanocable arrays exhibited 2.5 times higher photocurrent than planar Si/TiO_2 structures.[19] Based on these considerations, arrays of ZnO/CIS core/shell nanocables grown on transparent conducting substrates are believed to be a promising configuration for photovoltaic applications.

Many recent efforts have been devoted to the preparation of CIS nanostructures with various morphologies, such as nanocrystallites,[20,21] nanorods,[22,23] nanowires,[24,25] nanoparticles with trigonal pyramidal shape,[26] nanorings with hexagonal shape,[11] *etc*. However, to the best of our knowledge, the synthesis of CIS nanotubes has never been reported. Also there has been no report on the growth of 1D CIS nanoarrays on transparent conducting substrates. Herein, we report a simple and low-cost approach for synthesizing highly ordered arrays of CIS nanotubes and of ZnO/CIS core/shell nanocables with controllable Cu/In ratios on fluorine-doped tin oxide (FTO) or indium−tin oxide (ITO) coated glass substrates by using ZnO nanorod arrays as templates. Solar cells based on the arrays of ZnO/CIS core/shell nanocables were fabricated and characterized.

RESULTS AND DISCUSSION

Synthesis Scheme of CIS Nanotubes. The synthesis of arrays of ZnO nanorods/nanowires on various substrates has been successfully achieved *via* dip-coating under mild conditions.[17,27] Our strategy for the synthesis of the arrays of CIS nanotubes is illustrated in Scheme 1. The solubility product constant, K_{sp}, of ZnO (6.8×10^{-17}) is much larger than those of ZnSe (3.6×10^{-26}) and CuSe (7.94×10^{-49}). This implies that the arrays of ZnO nanorods can be used as sacrificial templates to synthesize more stable ZnSe by anion exchange and further convert into CuSe by cation exchange to obtain ZnO/CuSe core/shell nanocables. Arrays of ZnSe and CuSe nanotubes can also be prepared, respectively, by dissolving the inner ZnO nanorod cores of the ZnO/ZnSe and the ZnO/CuSe nanocables in an acetic acid solution. Arrays of CIS nanotubes can be prepared by using the CuSe nanotubes as self-sacrificial templates to react with In^{3+} *via* a polyol reduction process (the ZnO cores are slowly dissolved by the H^+ ions produced in the reaction if ZnO/CuSe core/shell nanocables are used instead).

Morphologies and Structures. Figure 1a and b shows, respectively, top- and cross-sectional views of SEM images of the highly ordered array of CIS 1D nanostructures with diameters of 50−100 nm and lengths of 2−3 μm prepared in an $InCl_3$ triethylene glycol (TEG) solution (2.0 mM) at 200 °C for 30 h. Some broken nanostructures (marked with arrows) in higher magnification SEM images in Figure 1c and d reveal these 1D closed-tip nanostructures have hollow interiors in the form of a sheath-like nanotube array. Figure 1e shows a high-resolution TEM image of a nanotube. Wall thickness of the polycrystalline nanotube is about 15 nm. The fringe spacing of 0.34 nm in Figure 1e matches well to the interplanar spacing of the {112} planes of the chalcopyrite $CuInSe_2$ crystal structure. Figure 1f shows a selected area electron-diffraction (SAED) pattern of a nanotube, indicating that the nanotube is polycrystalline.

The sample was further characterized by elemental electron energy loss spectroscopy (EELS) mappings. Figure 2b−d are, respectively, Cu, In, and Se elemental EELS mappings of a typical nanotube shown in Figure

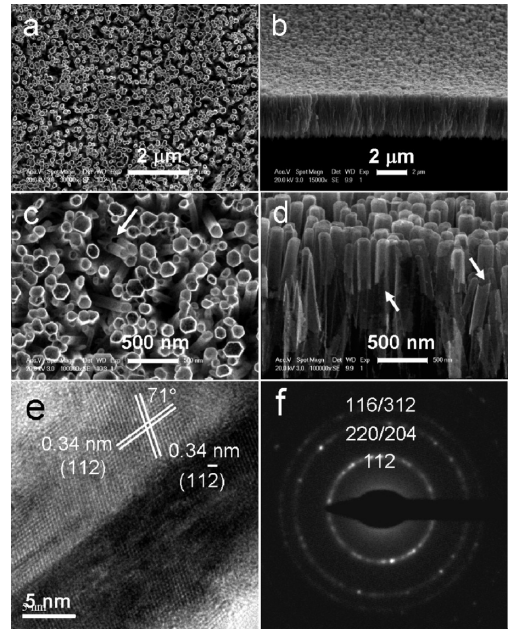

Figure 1. (a−d) SEM images of arrays of CIS nanotubes prepared in an $InCl_3$ TEG solution (2.0 mM) at 200 °C for 30 h; (e) a high-resolution TEM image; and (f) an SAED pattern of a tetragonal CIS nanotube.

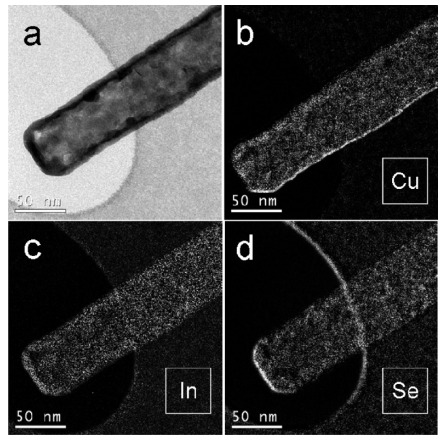

Figure 2. (a) TEM image of a CIS nanotube prepared in an $InCl_3$ TEG solution (2.0 mM) at 200 °C for 30 h, and (b−d) are, respectively, Cu, In, and Se elemental EELS mappings of the same region.

2a. The EELS results show that Cu, In, and Se are homogeneously distributed through the nanotubes.

It should point out that the ability to fine tune the Cu/In ratio in CIS is very important as the compound shows, respectively, p- and n-type conductivity when it is Cu or In rich.[28] In the present process, the Cu/In ratio can be controlled by the reaction time of CuSe in $InCl_3$ TEG solution. Figure S1 (in Supporting Information) shows energy-dispersive X-ray (EDX) spectra of CIS nanotubes obtained with different reaction durations. For each sample, EDX data were collected from at least five randomly selected areas to obtain an average composition. It can be seen that Cu-rich CIS nanotubes can be prepared with reaction times shorter than 20 h, while Cu-deficient CIS nanotubes are obtained when the reaction time is longer than 24 h.

Phase compositions of the samples were further examined by XRD analysis. Figure 3a shows an XRD spectrum of the nanotube array on ITO glass. All the diffraction peaks match well to those of tetragonal $CuInSe_2$ (JCPDF 75-0107), except the peaks marked with an asterisk, which comes from the ITO glass, as shown in Figure 3b. Figure 3c shows an XRD spectrum of the $CuInSe_2$ nanotube array grown on FTO glass. The peaks marked with a black dot come from FTO glass, as shown in Figure 3d. Abnormal intensity of the peak located at 26.6−26.7° in Figure 3c is attributed to the overlapping of the (112) peak of tetragonal $CuInSe_2$ and the (110) peak of tetragonal SnO_2 (JCPDF 41-1445).

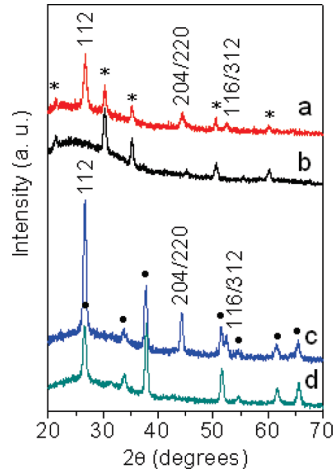

Figure 3. XRD spectra of (a) an array of CIS nanotubes on ITO glass; (b) an ITO-coated glass substrate; (c) an array of CIS nanotubes on FTO glass; and (d) a FTO-coated glass substrate.

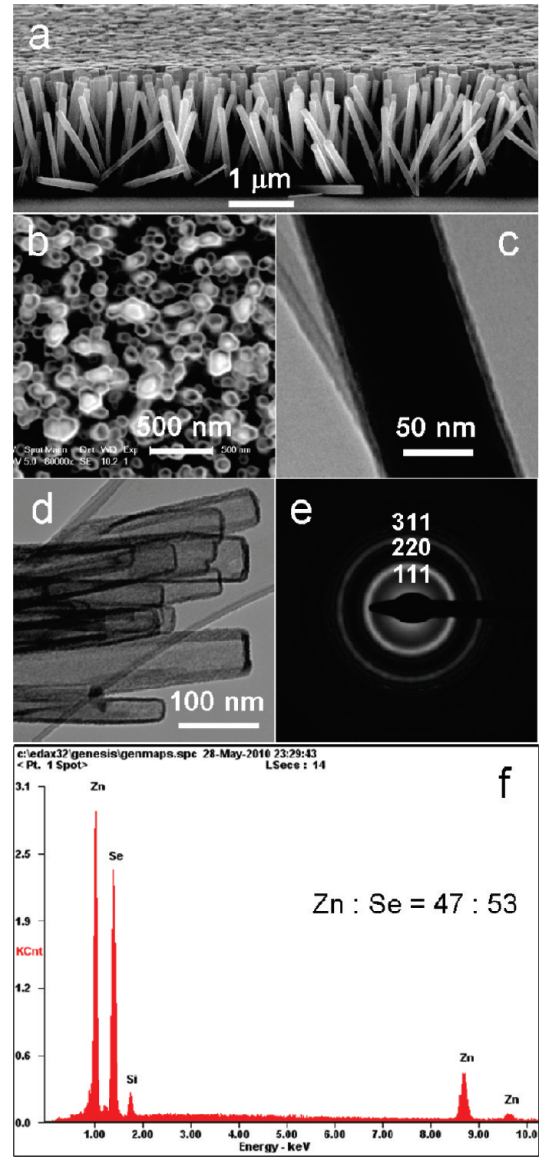

Figure 4. (a) SEM image of an array of ZnO nanorods; (b) SEM image of an array of ZnO/ZnSe core/shell nanocables; (c) TEM image of a ZnO/ZnSe core/shell nanocable; (d) TEM image of ZnSe nanotubes; (e) SAED pattern of a ZnSe nanotube; and (f) EDX spectrum of ZnSe nanotubes. For EDX measurement, the samples were removed from the FTO substrates and deposited on Si wafers. The Si peaks come from the Si wafers.

Formation Mechanisms. To understand the phase transformation and formation mechanisms of the CIS nanotubes array, we tracked the evolution process of the nanotube. Figure 4a shows a typical SEM image of an array of ZnO nanorods grown on FTO glass. The lengths

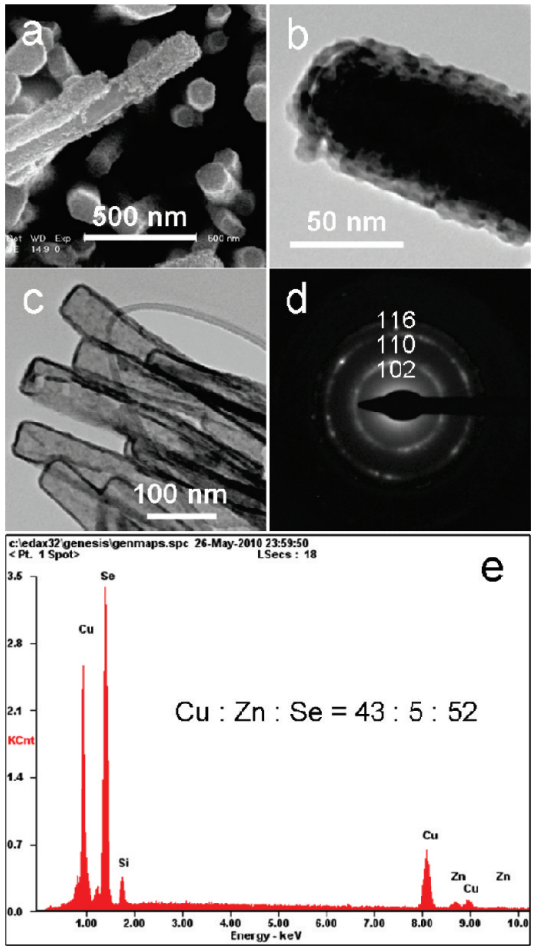

Figure 5. (a) SEM image and (b) TEM image of ZnO/CuSe core/shell nanocables; and (c) TEM image, (d) SAED pattern and (e) EDX spectrum of CuSe nanotubes.

of the ZnO nanorods typically range from 2−3 μm, and the diameters are in the range of 50−100 nm. Upon immersion into a Se^{2-} ion solution, ion-exchange reaction between Se^{2-} and ZnO will form a continuous layer of ZnSe on the nanorods resulting in the formation of ZnO/ZnSe core/shell nanocables (Figure 4b). A TEM image of the ZnO/ZnSe core/shell nanocable is shown in Figure 4c. Across the rod, the intensity profile shows a clear variation, and the edge surfaces shows lighter contrast. The formation of the sheath-like ZnSe nanotubes have been further confirmed by complete dissolution of the inner ZnO cores by immersing the array of ZnO/ZnSe core/shell nanocables in an acetic acid solution as shown in Figure 4d. An SAED pattern in Figure 4e reveals the cubic ZnSe nanotubes are polycrystalline. Figure 4f shows an EDX spectrum of the nanotubes demonstrates that the nanotubes only consist of zinc and selenium with an atomic ratio of 47:53.

When the array of ZnO/ZnSe core/shell nanocables was immersed in the Cu^{2+} ion solution, Cu^{2+} ions will replace the Zn^{2+} ions to form a CuSe sheath, resulting in the formation of ZnO/CuSe core/shell nanocables, as shown in Figure 5a and b, due to the smaller K_{sp} value of CuSe than that of ZnSe. After immersing the array of ZnO/CuSe core/shell nanocables in an acetic acid solution, CuSe nanotubes are obtained, as shown in Figure 5c. An SAED pattern in Figure 5d reveals the hexagonal CuSe nanotubes are polycrystalline. An EDX spectrum in Figure 5e reveals that the nanotubes consist of copper, zinc, and selenium with an atomic ratio of 43:5:52, suggesting the CuSe nanotubes mixed with a trace amount of residual ZnSe due to the incomplete replacement.

When such ZnO/CuSe core/shell nanocables were used as a precursor to react with enough In^{3+} ions in TEG, formation of CIS sheaths coupled with the gradual dissolution of ZnO cores is demonstrated, as shown in Figures S2 and S3 (Supporting Information). EDX results in Figure S1 (Supporting Information) reveal that no zinc was detected from the CIS sheaths after removing the ZnO cores in acetic acid solution. The CuSe (mixed with ZnSe) nanotube precursor is considered to undergo redissolution to enable the growth of a pure phase of CIS nanotubes. For mass conversion, the copper and selenium atomic ratio of 1:2 in the precursor will fulfill the requirements to prepare $CuInSe_2$. In our case, the Cu^{2+} ions are in surplus. These surplus copper ions and the unwanted zinc ions would diffuse outward from the nanotubes into the solvent during the conversion process.

In the present work, the formation of CIS nanotubes might have taken place *via* the following steps:

Preparation of Se^{2-} ion solution:

$$Se + 2BH_4^- \rightarrow Se^{2-} + H_2 + 2BH_3 \quad (1)$$

Formation of ZnSe sheaths:

$$ZnO + Se^{2-} + H_2O \rightarrow ZnSe + 2OH^- \quad (2)$$

Formation of CuSe sheaths:

$$ZnSe + Cu^{2+} \rightarrow CuSe + Zn^{2+} \quad (3)$$

Formation of the CIS nanotubes:

$$HO(CH_2CH_2O)_2CH_2CH_2OH \rightarrow HO(CH_2CH_2O)_2CH_2CHO + 2H \quad (4)$$

$$2CuSe + In^{3+} + H \rightarrow CuInSe_2 + Cu^{2+} + H^+ \quad (5)$$

Dissolution of the ZnO nanorods:

$$ZnO + 2H^+ \rightarrow Zn^{2+} + H_2O \quad (6)$$

When the arrays of the ZnO/CuSe core/shell nanocables react with enough In^{3+} in the TEG solvent, the conversion of CuSe to CIS is considered to result from a polyol reduction process.[29−32] TEG ($HO(CH_2CH_2O)_2CH_2CH_2OH$) has two hydroxy groups in each molecule. At high temperatures, a hydroxy group can denote two hydrogen atoms and convert to an analdehyde group.[33−35] The hydrogen atoms will denote electrons to become H^+ ions, and the cupric ions (Cu^{2+}) obtained the electrons are reduced to cuprous

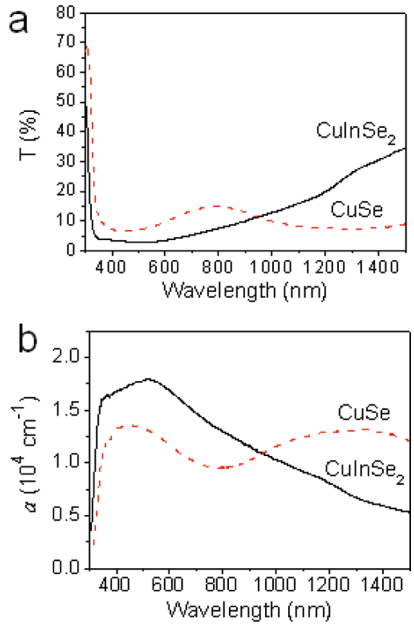

Figure 6. (a) Optical transmittance *T* (%) spectra of CuSe (red dashed line) and CIS (black solid line) nanotube arrays, and (b) UV−vis-NIR absorption spectra of the CuSe (red dashed line) and CIS (black solid line) nanotube arrays.

ions (Cu^+). At the same time, the cores of ZnO nanorods in the nanocables are simultaneously dissolved by the as-produced H^+ ions.

Optical Properties. Optical properties of the arrays of the CIS nanotubes and CuSe nanotubes were characterized by UV−vis-NIR spectrophotometry. Figure 6a shows optical transmittance spectra of the CIS (black solid line) and CuSe (red dashed line) nanotubes with length of ~2 μm revealing the transmittance of the CIS nanotubes is less than 8% in the visible region, which is much smaller than that of the CuSe nanotubes. In Figure 6b, the optical absorption spectrum of the CIS nanotubes shows a broad absorbance peak centered at ~516 nm, which is considered to originate from the nonbonding copper d localized states.[21] The array of CIS nanotubes displays absorption properties mainly over the visible region with a high absorption coefficient of the order of 10^4 cm^{-1}, which is comparable with the reported values of 10^4 and 10^5 cm^{-1} for thin films and the bulk sample, respectively.[36,37] The absorbance of the CuSe nanotubes shows a broad maximum from 400−500 nm and a local minimum at ~800 nm. It rises again over longer wavelengths in the NIR region, which is considered to be the result of free-carrier intraband absorbance.[38] This phenomenon is similar to those reported in CuSe thin film and $Cu_{2-x}S$ nanocrystals.[39,40]

Photoelectrochemical (PEC) Solar Cells. Using the nanoarray as the photoanode, we fabricated PEC solar cells to evaluate their PV performances. PV test for all cells, with an active cell area of 0.5 × 0.5 cm^2, was carried out under AM 1.5G simulated sunlight with an intensity of 100 mW cm^{-2}. Figure 7 shows the current density−voltage (*J*−*V*) characteristics of the cells. The cell based

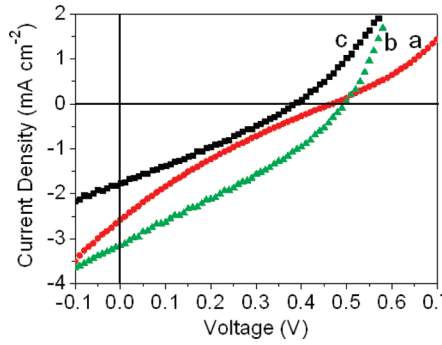

Figure 7. Current density−voltage (*J*−*V*) characteristics of PEC solar cells based on (a) ZnO/CuSe nanocables (0 h in TEG); (b) ZnO/$Cu_{1.57\pm0.10}In_{0.68\pm0.10}Se_2$ nanocables (2 h in TEG); and (c) ZnO/$Cu_{1.36\pm0.10}In_{0.89\pm0.10}Se_2$ nanocables (4 h in TEG).

on an array of ZnO/CuSe nanocables gives a short-circuit current density (J_{SC}) of 2.58 mA cm^{-2}, an open-circuit voltage (V_{OC}) of 0.46 V, and a fill factor (*FF*) of 0.21, yielding a power conversion efficiency (η) of 0.25%. When an array of ZnO/$Cu_{1.57\pm0.10}In_{0.68\pm0.10}Se_2$ core/shell nanocables is used as the photoanode, which was obtained by reacting ZnO/CuSe nanocables in the $InCl_3$ TEG solution for 2 h, the corresponding values are J_{SC} = 3.16 mA cm^{-2}, V_{OC} = 0.49 V, *FF* = 0.31, and η = 0.48%. Comparing the PV performances of the two cells, it is clear that, while the V_{OC} is similar, there is a significant improvement in both J_{SC} and *FF* for the cell based on ZnO/$Cu_{1.57\pm0.10}In_{0.68\pm0.10}Se_2$ core/shell nanocables, leading to about 2-fold increase in the power conversion efficiency. Increased content of CIS in the shell with a larger absorption coefficient in the visible region is favorable for PV performance. However, when the samples obtained by reacting ZnO/CuSe nanocables with $InCl_3$ in TEG solution for longer time, a decreased PV performance was observed. The solar cells based on an array of ZnO/$Cu_{1.36\pm0.10}In_{0.89\pm0.10}Se_2$ core/shell nanocables, which are obtained with reaction time of 4 h, yield a V_{OC} = 0.38 V, J_{SC} = 1.76 mA cm^{-2}, *FF* = 0.28, and η = 0.19%. The reason for this decreased PV performance is considered to be the result of the decreased p−n junction areas in the nanocables as the ZnO cores are gradually dissolved in the CIS evolution process, which is demonstrated by XRD results in Figure S2 and SEM images in Figure S3 (Supporting Information). No PV performance of the devices is observed when the ZnO cores are completely dissolved. Compared with the traditional planar CIS solar cells with a typical V_{OC} value of 0.3−0.4 V,[10−12] the V_{OC} of our device is greatly improved, although the J_{SC} is low. In our core/shell nanocable configuration, when electron−hole pairs are generated by visible light excitation in p−n junction, the photoelectrons can be transferred to the conduction band of the ZnO nanorods without the presence of grain boundaries, which facilitates a charge separation process of electron−hole pairs before they recombine. On the other hand, it has been reported that the electrolyte used here can cause mild corrosion to ZnO.[41]

This might be a possible cause for the lower J_{SC} in the present solar cells. Our devices provide a baseline performance and demonstrate as a proof of concept that such ZnO/CIS core/shell nanocables can be used in PV devices. The PV performance can be improved in several ways, including synthesizing ZnO/CIS nanocables with a solid ZnO core, incorporating Ga into $CuInSe_2$ to form $CuIn_xGa_{1-x}Se_2$ with a suitable bandgap for longer wavelength absorption, and coating a CdS buffer layer in the ZnO−CISG solar cell for better energy level alignment. All these are ongoing for further studies.

CONCLUSIONS

Arrays of copper indium selenide (CIS) nanotubes with controllable Cu/In ratios were directly grown on transparent conducting substrates with a low-cost, low-temperature solution process by using ZnO nanorods as sacrificial templates. Large differences in the solubility products of the source and the product materials facilitate efficient ion exchanges for the chemical conversion. The array of CIS nanotubes was shown to have an absorption coefficient of 10^4 cm^{-1} in the visible region which is much higher than that of CuSe, resulting in about a 2 times increase in the power conversion efficiency in photoelectrochemical (PEC) solar cells. Furthermore, this synthetic strategy may be extended to fabricate other functional I−III−VI one-dimensional nanoarrays on transparent conducting substrates, which is beneficial for their applications in various optoelectronic devices.

EXPERIMENTAL SECTION

Synthesis of Arrays of ZnO Nanorods on ITO/FTO-Coated Glasses. Arrays of ZnO nanorods on ITO or FTO coated glasses were prepared by a dip-coating method.[17,27] ITO or FTO glasses were first cleaned with acetone, ethylene glycol, and ethanol by ultrasonication for several times. The substrate was wetted with a drop of zinc acetate ethanol solution (5.0 mM) and then dried with a nitrogen blow. This coating step was repeated three to five times. The substrate was then heated at 350 °C in air for 20 min to form a layer of ZnO seeds. ZnO nanorods were then grown by immersing the seeded substrates in an aqueous solution containing zinc nitrate hydrate (25.0 mM), hexamethylenetetramine (25.0 mM), and polyethylenimine (5.0 mM) at 90 °C for 6−12 h. The samples were then taken out from the solution, washed with deionized water and absolute ethanol, and then dried in air.

Synthesis of Arrays of ZnO/ZnSe Core/Shell Nanocables and ZnSe Nanotubes. A Se^{2-} source solution was first prepared by dissolving 0.015 g of Se and 0.05 g of $NaBH_4$ in 30 mL of water. Arrays of ZnO/ZnSe core/sheath nanocables were prepared by immersing the ZnO nanorod arrays in the Se^{2-} source solution and kept at 50 °C for 3 h. This process was repeated two times. The prepared ZnO/ZnSe core/shell nanocable arrays were then immersed in an acetic acid solution (5 wt %) for about 20 min to completely remove the inner ZnO cores to produce arrays of ZnSe nanotubes. The samples were then washed with deionized water and absolute ethanol and finally dried in air.

Synthesis of Arrays of ZnO/CuSe Core/Shell Nanocables and CuSe Nanotubes. In 20 mL of triethylene glycol (TEG), 1.0 mmol of $Cu(NO_3)_2 \cdot 3H_2O$ was first dissolved. Arrays of ZnO/ZnSe core/shell nanocables were immersed in the above solution and kept for 3−6 h at room temperature to prepare arrays of ZnO/CuSe core/shell nanocables. After immersing the obtained arrays of ZnO/CuSe core/shell nanocables in an acetic acid solution (5 wt %) for about 20 min, arrays of ZnSe nanotubes were prepared. The samples were then washed with deionized water and absolute ethanol and finally dried in air.

Synthesis of Arrays of ZnO/CIS Nanocables and CIS Nanotubes. In a Teflon-lined stainless steel autoclave, 0.02−0.04 mmol of $InCl_3$ was first dissolved in 20 mL of TEG. Arrays of ZnO/CuSe core/shell nanocables were immersed in the above solution. The autoclave was then sealed and maintained at 200 °C. Typically, arrays of ZnO/CIS nanocables were obtained in 2−4 h, while arrays of CIS nanotubes were obtained when the reaction duration is extended to 12−30 h. After being naturally cooled to room temperature, the samples were washed with deionized water and then absolute ethanol for several times and finally dried in air.

Fabrication of Solar Cells. Arrays of ZnO/CIS core/shell nanocables and ZnO/CuSe nanocables grown on FTO glasses were first annealed at 400 °C in argon for 30 min. The samples were then sandwiched and bonded with a platinum-coated (~30 nm) FTO counter electrode. The two electrodes were separated by a 60 μm thick polypropylene spacer, and the internal space of the cells was filled with a liquid electrolyte (0.1 M LiI, 50 mM I_2, and 0.6 M DMPII (Solaronix)) in acetonitrile by capillary action. Solar cells were immediately tested under AM 1.5G simulated sunlight. The active area of the solar cells was 0.5 × 0.5 cm^2.

Characterization of Samples. As-prepared samples were characterized with X-ray diffraction (XRD) using a Siemens D-500 diffractometer with Cu Kα radiation. Scanning electron microscopy (SEM) and transmission electron microscopy (TEM) were carried out, respectively, with a Philips XL30 FEG SEM and a Philips CM 20 (or a Philips CM200 FEG or a JEOL JEM-2100F, all operated at 200 kV) TEM. Electron energy loss spectroscopy (EELS) data were acquired with a Gatan Tridiem imaging filter attached to the JEOL TEM. Absorption spectra were recorded with a lambda-750 UV−vis-NIR spectrophotometer. Current density−voltage (*J*−*V*) characteristics of the solar cells were measured under AM 1.5G illumination with an intensity of 100 mW cm^{-2}.

Acknowledgment. This project has been financially supported by the Research Grants Council of HKSAR (no. CityU 101910) and the National 973 program (2009CB623703), MOST, People's Republic of China. The authors thank Mr. T. F. Hung for TEM and EELS characterization.

Supporting Information Available: EDX and XRD spectra and SEM images for the evolution process of the arrays of CIS nanotubes from ZnO/CuSe nanocables grown on FTO-coated glasses. This material is available free of charge *via* the Internet at http://pubs.acs.org.

REFERENCES AND NOTES

1. Dhere, N. G. Toward GW/Year of CIGS Production within the Next Decade. *Sol. Energy Mater. Sol. Cells* **2007**, *91*, 1376–1382.
2. Compaan, A. D. Photovoltaics: Clean Power for the 21st Century. *Sol. Energy Mater. Sol. Cells* **2006**, *90*, 2170–2180.
3. Hegedus, S. S.; Shafarman, W. N. Thin-Film Solar Cells: Device Measurements and Analysis. *Prog. Photovoltaics: Res. Appl.* **2004**, *12*, 155–176.
4. Chopra, K. L.; Paulson, P. D.; Dutta, V. Thin-Film Solar Cells: An Overview. *Prog. Photovoltaics: Res. Appl.* **2004**, *12*, 69–92.
5. Contreras, M. A.; Egaas, B.; Ramanathan, K.; Hiltner, J.; Swartzlander, A.; Hasoon, F.; Noufi, R. Progress toward 20% Efficiency in Cu(In, Ga)Se_2 Polycrystalline Thin-Film Solar Cells. *Prog. Photovoltaics: Res. Appl.* **1999**, *7*, 311–316.
6. Repins, I.; Contreras, M. A.; Egaas, B.; DeHart, C.; Scharf, J.; Perkins, C. L.; To, B. 19 · 9%-Efficient ZnO/CdS/$CuInGaSe_2$ Solar Cell with 81.2% Fill Factor. *Prog. Photovoltaics: Res. Appl.* **2008**, *16*, 235–239.

7. Ward, J. S.; Ramanathan, K.; Hasoon, F. S.; Coutts, T. J.; Keane, J.; Contreras, M. A.; Moriarty, T.; Noufi, R. A 21.5% Efficient Cu(In, Ga)Se_2 Thin-Film Concentrator Solar Cell. *Prog. Photovoltaics: Res. Appl.* **2002**, *10*, 41–46.
8. Ramanathan, K.; Contreras, M. A.; Perkins, C. L.; Asher, S.; Hasoon, F. S.; Keane, J.; Young, D.; Romero, M.; Metzger, W.; Noufi, R.; Ward, J.; Duda, A. Properties of 19.2% Efficiency ZnO/CdS/$CuInGaSe_2$ Thin-Film Solar Cells. *Prog. Photovoltaics: Res. Appl.* **2003**, *11*, 225–230.
9. Dhere, N. G. Present Status and Future Prospects of CIGSS Thin Film Solar Cells. *Sol. Energy Mater. Sol. Cells* **2006**, *90*, 2181–2190.
10. Panthani, M. G.; Akhavan, V.; Goodfellow, B.; Schmidtke, J. P.; Dunn, L.; Dodabalapur, A.; Barbara, P. F.; Korgel, B. A. Synthesis of $CuInS_2$, $CuInSe_2$, and $Cu(In_xGa_{1-x})Se_2$ (CIGS) Nanocrystal "Inks" for Printable Photovoltaics. *J. Am. Chem. Soc.* **2008**, *130*, 16770–16777.
11. Guo, Q. J.; Kim, S. J.; Kar, M.; Shafarman, W. N.; Birkmire, R. W.; Stach, E. A.; Agrawal, R.; Hillhouse, H. W. Development of $CuInSe_2$ Nanocrystal and Nanoring Inks for Low-Cost Solar Cells. *Nano Lett.* **2008**, *8*, 2982–2987.
12. Guo, Q. J.; Ford, G. M.; Hillhouse, H. W.; Agrawal, R. Sulfide Nanocrystal Inks for Dense $Cu(In_{1-x}Ga_x)(S_{1-y}Se_y)_2$ Absorber Films and Their Photovoltaic Performance. *Nano Lett.* **2009**, *9*, 3060–3065.
13. Tsakalakos, L.; Balch, J.; Fronheiser, J.; Shih, M.-Y.; LeBoeuf, S. F.; Pietrzykowski, M.; Codella, P. J.; Korevaar, B. A.; Sulima, O.; Rand, J.; Davuluru, A.; Rapol, U. Strong Broadband Optical Absorption in Silicon Nanowire Films. *J. Nanophotonics* **2007**, *01*, 013552.
14. Kayes, B. M.; Atwater, H. A.; Lewis, N. S. Comparison of the Device Physics Principles of Planar and Radial p-n Junction Nanorod Solar Cells. *J. Appl. Phys.* **2005**, *97*, 114302.
15. Tian, B.; Zheng, X.; Kempa, T. J.; Fang, Y.; Yu, N.; Yu, G.; Huang, J.; Lieber, C. M. Coaxial Silicon Nanowires as Solar Cells and Nanoelectronic Power Sources. *Nature* **2007**, *449*, 885–889.
16. Garnett, E. C.; Yang, P. D. Silicon Nanowire Radial p-n Junction Solar Cells. *J. Am. Chem. Soc.* **2008**, *130*, 9224–9225.
17. Law, M.; Greene, L. E.; Johnson, J. C.; Saykally, R.; Yang, P. D. Nanowire Dye-Sensitized Solar Cells. *Nat. Mater.* **2005**, *4*, 455–459.
18. Wang, X.; Zhu, H.; Xu, Y.; Wang, H.; Tao, Y.; Hark, S.; Xiao, X.; Li, Q. Aligned ZnO/CdTe Core/Shell Nanocable Arrays on Indium Tin Oxide: Synthesis and Photoelectrochemical Properties. *ACS Nano* **2010**, *4*, 3302–3308.
19. Hwang, Y. J.; Boukai, A.; Yang, P. D. High Density n-Si/n-TiO_2 Core/Shell Nanowire Arrays with Enhanced Photoactivity. *Nano Lett.* **2009**, *9*, 410–415.
20. Li, B.; Xie, Y.; Huang, J. X.; Qian, Y. T. Synthesis by a Solvothermal Route and Characterization of $CuInSe_2$ Nanowhiskers and Nanoparticles. *Adv. Mater.* **1999**, *11*, 1456–1459.
21. Xiao, J. P.; Xie, Y.; Xiong, Y. J.; Tang, R.; Qian, Y. T. A Mild Solvothermal Route to Chalcopyrite Quaternary Semiconductor $CuIn(Se_xS_{1-x})_2$ Nanocrystallites. *J. Mater. Chem.* **2001**, *11*, 1417–1420.
22. Jiang, Y.; Wu, Y.; Mo, X.; Yu, W. C.; Xie, Y.; Qian, Y. T. Elemental Solvothermal Reaction to Produce Ternary Semiconductor $CuInE_2$ (E = S, Se) Nanorods. *Inorg. Chem.* **2000**, *39*, 2964–2965.
23. Yang, Y.-H.; Chen, Y.-T. Solvothermal Preparation and Spectroscopic Characterization of Copper Indium Diselenide Nanorods. *J. Phys. Chem. B* **2006**, *110*, 17370–17374.
24. Schoen, D. T.; Peng, H. L.; Cui, Y. Anisotropy of Chemical Transformation from In_2Se_3 to $CuInSe_2$ Nanowires through Solid State Reaction. *J. Am. Chem. Soc.* **2009**, *131*, 7973–7975.
25. Xu, J.; Lee, C.-S.; Tang, Y.-B.; Chen, X.; Chen, Z.-H.; Zhang, W.-J.; Lee, S.-T.; Zhang, W. X.; Yang, Z. H. Large-Scale Synthesis and Phase Transformation of CuSe, $CuInSe_2$, and $CuInSe_2$/$CuInS_2$ Core/Shell Nanowire Bundles. *ACS Nano* **2010**, *4*, 1845–1850.
26. Koo, B.; Patel, R. N.; Korgel, B. A. Synthesis of $CuInSe_2$ Nanocrystals with Trigonal Pyramidal Shape. *J. Am. Chem. Soc.* **2009**, *131*, 3134–3135.
27. Greene, L. E.; Law, M.; Tan, D. H.; Montano, M.; Goldberger, J.; Somorjai, G.; Yang, P. D. General Route to Vertical ZnO Nanowire Arrays Using Textured ZnO Seeds. *Nano Lett.* **2005**, *5*, 1231–1236.
28. Courtel, F. M.; Paynter, R. W.; Marsan, B.; Morin, M. Synthesis, Characterization, and Growth Mechanism of n-Type $CuInS_2$ Colloidal Particles. *Chem. Mater.* **2009**, *21*, 3752–3762.
29. Skrabalak, S. E.; Wiley, B. J.; Kim, M.; Formo, E. V.; Xia, Y. N. On the Polyol Synthesis of Silver Nanostructures: Glycolaldehyde as a Reducing Agent. *Nano Lett.* **2008**, *8*, 2077–2081.
30. Li, C.; Shuford, K. L.; Chen, M.; Lee, E. J.; Cho, S. O. A Facile Polyol Route to Uniform Gold Octahedra with Tailorable Size and Their Optical Properties. *ACS Nano* **2008**, *2*, 1760–1769.
31. Zheng, L.; Xu, Y.; Song, Y.; Wu, C. Z.; Zhang, M.; Xie, Y. Nearly Monodisperse $CuInS_2$ Hierarchical Microarchitectures for Photocatalytic H_2 Evolution under Visible Light. *Inorg. Chem.* **2009**, *48*, 4003–4009.
32. Orel, Z. C.; Anžlovar, A.; Dražić, G.; Žigon, M. Cuprous Oxide Nanowires Prepared by an Additive-Free Polyol Process. *Cryst. Growth Des.* **2007**, *7*, 453–458.
33. Kawai, F.; Kimura, T.; Fukaya, M.; Tani, Y.; Ogata, K.; Ueno, T.; Fukami, H. Bacterial Oxidation of Polyethylene Glycol. *Appl. Environ. Microbiol.* **1978**, *35*, 679–684.
34. Zhang, W. X.; Wang, C.; Zhang, X. M.; Xie, Y.; Qian, Y. T. Low Temperature Synthesis of Nanocrystalline Mn_3O_4 by a Solvothermal Method. *Solid State Ionics* **1999**, *117*, 331–335.
35. Zheng, Y. H.; Cheng, Y.; Wang, Y. S.; Zhou, L. H.; Bao, F.; Jia, C. Metastable γ-MnS Hierarchical Architectures: Synthesis, Characterization, and Growth Mechanism. *J. Phys. Chem. B* **2006**, *110*, 8284–8288.
36. Yüksel, Ö. F.; Başol, B. M.; Şafak, H.; Karabiyik, H. Optical Characterization of $CuInSe_2$ Thin Films Prepared by Two-Stage Process. *Appl. Phys. A: Mater. Sci. Process.* **2001**, *73*, 387–389.
37. Rockett, A.; Birkmire, R. W. $CuInSe_2$ for Photovoltaic Application. *J. Appl. Phys.* **1991**, *70*, R81–R97.
38. García, V. M.; Nair, P. K.; Nair, M. T. S. Copper Selenide Thin Films by Chemical Bath Deposition. *J. Cryst. Growth* **1999**, *203*, 113–124.
39. Pejova, B.; Grozdanov, I. Chemical Deposition and Characterization of Cu_3Se_2 and CuSe Thin Films. *J. Solid State Chem.* **2001**, *158*, 49–54.
40. Zhao, Y. X.; Pan, H. C.; Lou, Y. B.; Qiu, X. F.; Zhu, J. J.; Burda, C. Plasmonic $Cu_{2-x}S$ Nanocrystals: Optical and Structural Properties of Copper-Deficient Copper (I) Sulfides. *J. Am. Chem. Soc.* **2009**, *131*, 4253.
41. Ke, L.; Dolmanan, S. B.; Shen, L.; Pallathadk, P. K.; Zhang, Z.; Lai, D. M. Y.; Liu, H. Degradation Mechanism of ZnO-Based Dye-Sensitized Solar Cells. *Sol. Energy Mater. Sol. Cells* **2010**, *94*, 323–326.